CONF-8307101--2

MEASUREMENT OF INGOT-CRUCIBLE BOUNDARY CONDITIONS DURING VACUUM ARC REMELTING†

L. A. Bertram and F. J. Zanner
Sandia National Laboratories*

SAND--83-0150C

DE84 008851

Summary

This study is part of an ongoing program aimed at characterization of macrosegregation in vacuum consumable arc remelting. Such macrosegregation is attributed to fluid flow in the melt pool and the solidifying zone atop the ingot, so its prediction requires precise determination of the thermal conditions which shape these zones. These conditions in turn result from the complicated processes which fix the heat flux distribution between ingot and crucible wall. The experiments reported here attempt measurement of this flux distribution on the outside of the crucible wall, and calculation of the inside flux from that data. Measurements are made with an array of 40 stainless steel sheathed, electrically insulated, cromel/alumel thermocouples imbedded in the outside surface of the 203 mm ID copper crucible. In one melt two Ta sheathed, electrically insulated, W-5Re/W-26Re thermocouples were imbedded in the inside wall as well. Simultaneous measurements were made on total input power to the furnace, and by monitoring coolant flowrate and temperature rise, of total coolant power extracted. Major interest is on the 15-20 min. duration period of quasisteady melting conditions at constant melt current of 6 kA. Checks on ingot length (and thus, on meltrate) were obtained at intervals by driving the electrode down to the pool surface, causing a "ram short." Results for two melts of U-6w/oNb give meltrates which agree to about 7 percent, and indicate that about half the coolant power is heat deposited above the pool surface, and half below. The ingot-crucible contact extends from 50-75 cm below the pool surface. Measured inside temperature rises are compatible with inside temperature inferred by solving the inverse heat flow problem for the crucible wall, but noise levels preclude assigning significance to this agreement.

†Presented at Engineering Foundation Conference on "Modeling of Casting and Welding Processes", Henniker, NH, July-August 1983.

*Sandia National Laboratories is operated for the U.S. Department of Energy under contract DE-AC04-76DP00789.

Introduction

Vaccum consumable arc remelting is essentially a controlled solidification process designed to produce near-steady conditions in large cylindrical ingots. The process is carried out in a water cooled, copper walled vacuum crucible by melting a consumable electrode (cathode) by arc heating (Figure 1). The total electrical input power is partitioned between cathode heating, anode heating, and residual heat content in the ingot. Our aim here is determination of these energy partitions as well as characterization of the heat transfer between the ingot lateral surface and the inside of the crucible wall.

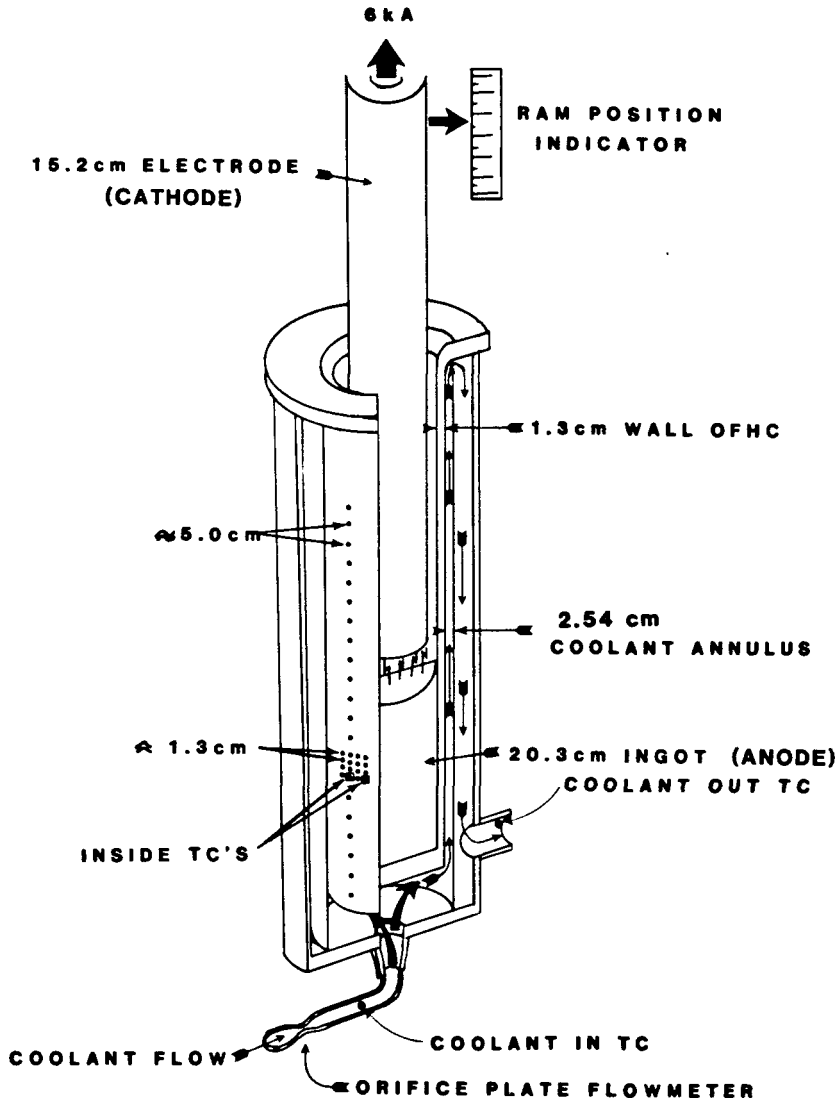

Figure 1. Schematic of instrumented Cu crucible used in U-6w/oNb melts.

The ingot-crucible boundary condition is of particular interest because of its importance to numerical simulation of solidification conditions in the ingot (1), (2). Since heat is deposited on the pool surface by inflow of molten metal and by anode arc processes, the pool must transfer this heat to the crucible via their mutual contact zone. When this contact zone is confined to a small region near the meniscus of the pool, a quite constricted heat flow path results. Solidification conditions in such a case would have to be quite sensitive to details of such a contact zone. Therefore, a central question to be answered by measurement, is the length scale of contact.

Measurements described in the second section were undertaken for two nominally identical electrodes of U-6w/oNb alloy. Crucible wall temperature was measured inside and outside the crucible wall, and then analyzed as described in the third section to give estimates of the inside quasisteady temperature and flux distributions. Quasisteady conditions would correspond to conditions in an infinitely long crucible after an infinite transient time had elapsed. The results of this analysis and conclusions drawn from it are presented in the final section.

Experimental Procedures

The two melts analyzed in this paper consisted of about 30 minute duration remelts of 152 mm (6 in) nominal diameter electrodes into 203 mm (8 in) nominal diameter ingots weighing approximately 330 kg. Melting current was held constant (except for a short startup procedure of about one minute) at 6 kA, resulting in nominal voltages of 24-26 V for the first case (designated M 68) and 26-30 V for the second (M 70). Furnace pressure ranged from 0.27 to 1.06 Pa (2-8 microns) for both melts; leak rates were less than 3×10^{-4} Pa/s (8 micron/hr). Coolant (50 percent Glycol, 50 percent water) flowrate was steady at 3×10^{-4} m^3/s (50 gpm) for M 68 and at 5.4×10^{-4} m^3/s (90 gpm) for M 70.

A description of the furnace and its instrumentation is given in Refs. (3) and (4). Additional instrumentation for the present work included a data logger with RS 232 interface to a minicomputer for the thermocouple data. The crucible exterior thermocouples were cromel/alumel, sheathed with 304 stainless steel, and of 0.66 mm diameter. Two 0.66 mm diameter, Ta sheathed, W-5Re/W-26Re thermocouples were used to obtain inside temperature on M 68. All thermocouples were electrically isolated and each was sampled by the data logger at 25s (M 68) or 23s (M 70) intervals.

The placement of thermocouples on the crucible wall is indicated in Figure 1. The vertical line of 20 thermocouples was spaced at 50.8 mm (2 in) intervals; the dense 4 x 4 array had 12.7 mm (1/2 in) vertical and horizontal spacings. This array was placed about 1-1/2 diameters above the stool to assure quasisteady melting conditions at the time of pool passage.

Each thermocouple was imbedded flush with the crucible surface by milling a slot 0.68 mm wide into the copper, inserting the thermocouple tip, and then peening the copper edges of the slot over it. Leads were routed through holes drilled in the crucible flange and sealed watertight. To prevent excess flexing in the flowing coolant, leads for M 68 were secured to the crucible at 155 mm spacings by fiberglass tape. Because analysis of data indicated that a combination of low coolant flowrate and interference of this surface roughness with heat transfer could result in boiling of the coolant, both flowrate and securing of leads were changed for M 70. Its flowrate was nearly doubled, and 0.25 mm wires were used at 200 mm spacing to secure leads.

The inside thermocouple leads in M 68 were peened into milled slots along their entire lengths. Particular care was taken to assure intimate contact between sheath tip and the crucible wall.

Synchronization of electrical and temperature records was obtained by writing time marks from quartz oscillators onto the magnetic tape records of the former and the digital records of the latter. Constancy of coolant flowrate was monitored by an orifice plate flowmeter. Electrode gap was manually controlled, using "ram short" procedures to determine actual interelectrode gap (4). At the end of the melt, power was turned off without any "hot top" procedure. Final ingot length L_f was measured after the ingot was removed from the furnace.

Analysis

There are two major experimental shortcomings in the procedure described above. First, the boundary condition of interest is the simplest; namely, the quasisteady melt condition. Direct observation would require an infinite crucible. Second, temperature data can only be reliably obtained with high resolution on the outside of the crucible, so inside conditions can be obtained only by solving an ill-posed problem (inverse heat flow). The inside thermocouple data can at best serve only as a consistency check and constraint on this process, except under exceptionally low-noise conditions of melting.

These issues can be seen by considering heat flow through a section of the crucible wall of length L and thickness H, as seen in coordinates moving upward with the pool surface (Figure 2). In these coordinates, the copper of the wall appears to move from right to left at velocity U_I (speed of ingot growth). The length L of the region of interest is chosen to enclose the significant heat flux.

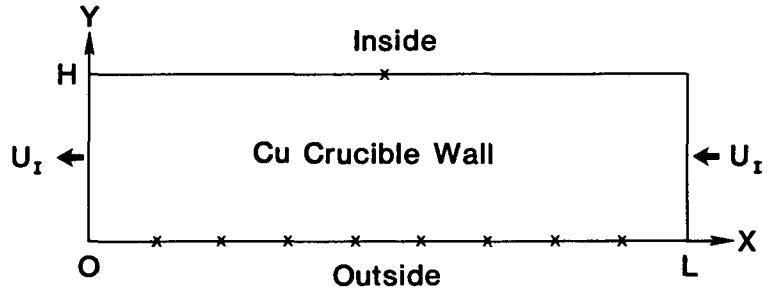

Figure 2. Section of crucible wall in coordinates moving with pool (schematic). Curvature is neglected in this approximation. Thermocouples indicated by "x".

In such coordinates, the constant property heat conduction equation is (neglecting wall curvature)

$$- U_I \frac{\partial T}{\partial x} = \kappa\left(\frac{\partial^2 T}{\partial x^2} + \frac{\partial^2 T}{\partial y^2}\right) \tag{1}$$

where κ is the thermal diffusivity of OFHC Cu, about 1 cm^2/s. By substituting the expression

$$T(x,y) = \exp\,(-U_I x/2\kappa)\ \Theta(x,y), \tag{2}$$

eq. (1) becomes a Helmholtz equation for $\Theta(x,y)$:

$$\frac{\partial^2 \Theta}{\partial x^2} + \frac{\partial^2 \Theta}{\partial y^2} - \frac{U_I^2}{4\kappa^2}\,\Theta = 0. \tag{3}$$

It follows from eqs. (2) and (3) that the temperature distribution is characterized by a length scale $L_T = 2\kappa/U_I \sim 30$ cm for OFHC Cu in quasisteady melting. This suggests that measurements would have to include at least 1.0 m of distance L in Figure 2 to be certain of capturing the quasisteady heat flux distribution. Such a length is not feasible for the electrodes and crucibles available, so the thermocouples had to be arranged in such a way that different segments of this quasisteady pulse $T(x,y = 0)$ could be captured by different thermocouples as shown in Figure 3.

Two methods were used to assemble the quasisteady pulse composite $T_c(t^*)$. First, the traces $T_i(t)$ can be assembled in a variation-minimizing way, and the time offsets between channels required to do this can be noted. This corresponds to the process depicted in Figure 3; applied to real data, it yields the results shown in Figure 4. The relative time scale t^* was chosen as the time scale of the thermocouple 1, the thermocouple furthest up the crucible. This scale is then related to the quartz oscillator scale by requiring that

$$x_p(t^*_{off}) = L_f \tag{4}$$

hold, where x_p is the time-dependent ingot length and L_f is the final ingot length, and "off" refers to power off time. Since the quartz clock time t_{off} is known with great precision from the furnace electrical signals (current and voltage), eq. (4) fixes t^* in relation to the origin of t, time after power on.

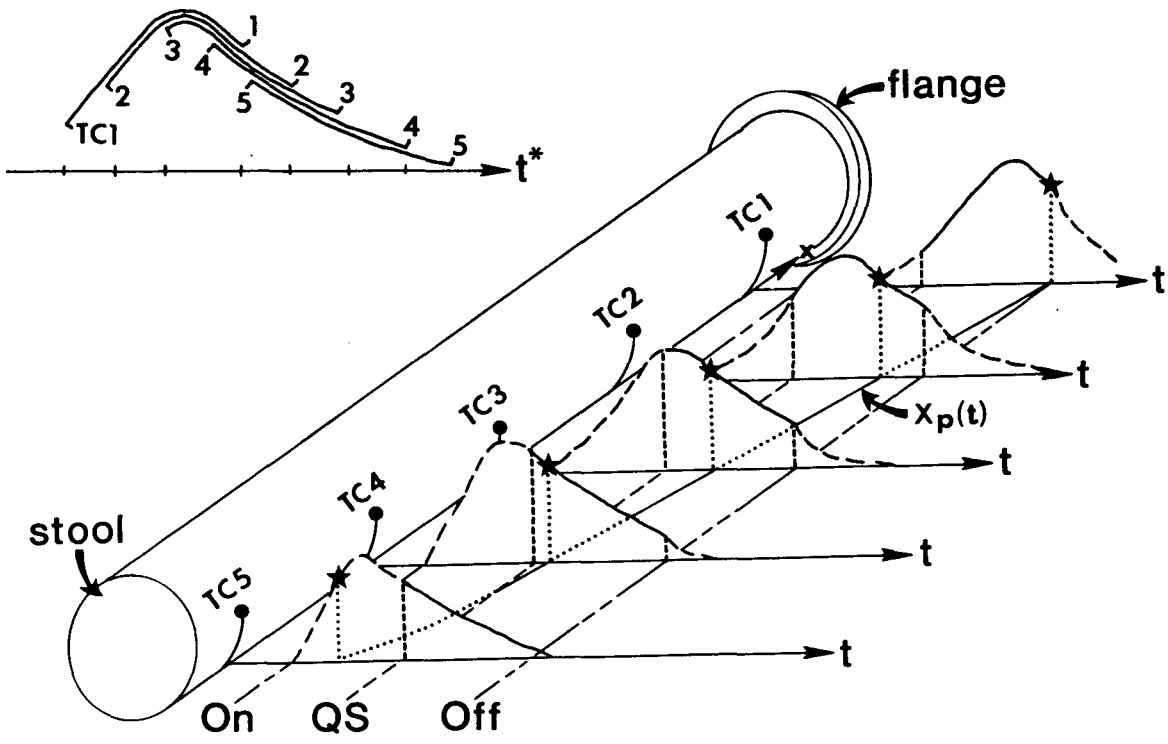

Figure 3. Assembly of individual thermocouple (TC) histories $T_i(t)$ into composite quasisteady heat pulse $T_c(t^*)$-schematic. Power applied at "ON", removed at "OFF"; stars denote time of pool arrival at TC with index i, and $x_p(t)$ is pool position (ingot length) at time t. Quasisteady conditions begin at "QS"; solid line portions of individual histories are quasisteady data and broken line portions are transients associated with power on and power off. Note that a thermocouple too near the stool could be cooled by axial conduction and never achieve quasisteady conditions.

A second determination $x_p(t)$ is made from measurements of the electrode position during ram shorts. This is transformed into pool position by

$$x_p(t) = x_o + \frac{L_f}{x_r(t_{off}) - x_o} \; x_r(t) \qquad (5)$$

where $x_r(t)$ is the position of the ram at time t; $x_o = x_r(0)$, and is given by

$$x_o = x_r(t_{on}) + h_{st} - \left(\frac{V_{st}}{\pi R^2}\right), \qquad (5a)$$

where h_{st} and V_{st} are, respectively, the unmelted height of the striker block and its volume. R is 1/2 (crucible ID).

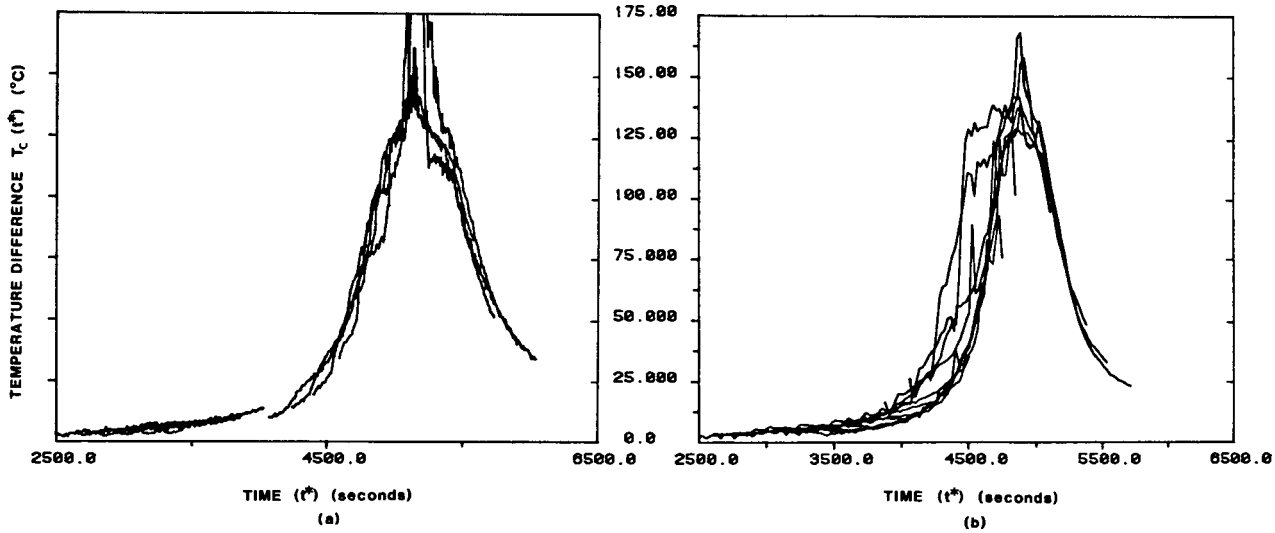

Figure 4. Composite $T_c(t^*)$ construction from individual thermocouple traces $T_i(t)$ for (a) M 68 and (b) M 70. T_c (t^*) is temperature difference (°C) between outside crucible wall and coolant. Coolant bulk temperature $T_\infty(x)$ is given as:

$$T_\infty(x) = T_{out}(t) - \alpha(x)\left(T_{out}(t) - T_{in}(t)\right)$$

in terms of coolant inflow and outflow temperatures and the fraction $\alpha(x)$ of the heat pulse already past at station x:

$$\alpha(x) = \int_{-\infty}^{x} h\, T_c(x)dx \Big/ \int_{-\infty}^{\infty} h\, T_c(x)dx.$$

where h is the coolant film coefficient. This assembly process requires iteration until $T_\infty(x)$ and $T_c(t^*)$ converge simultaneously. Since $T_\infty(x)$ varies by about ± 3°C about a mean of 19°C, the $T_c(t^*)$ curves can be read as roughly (wall temperature − 19°C). Since coolant boils at about 143°C, the "noise" near the heat pulse peaks represents temperature excursions (increases) due to boiling.

Since both $x_p(t)$ measurements are constrained to match the final ingot length, their values must be quite similar as seen in Figure 5. However, the high noise level in M 68 thermal data, probably due to coolant boiling, renders its thermally-determined $x_p(t)$ less reliable than the ram short data. Therefore, the constant velocity curve fit to the M 68 data in Figure 5 favors the ram data. This also proves to be more consistent with the operator's reported time of first melt (intersection of broken line with striker line at lower left). In the M 70 data, open circles and x's in the figure, this conflict does not appear--ram and thermal data are quite consistent. The slopes of the constant velocity curve fits gave 0.033 cm/s and 0.036 cm/s for M 68 and M 70 respectively, for the derived U_I values.

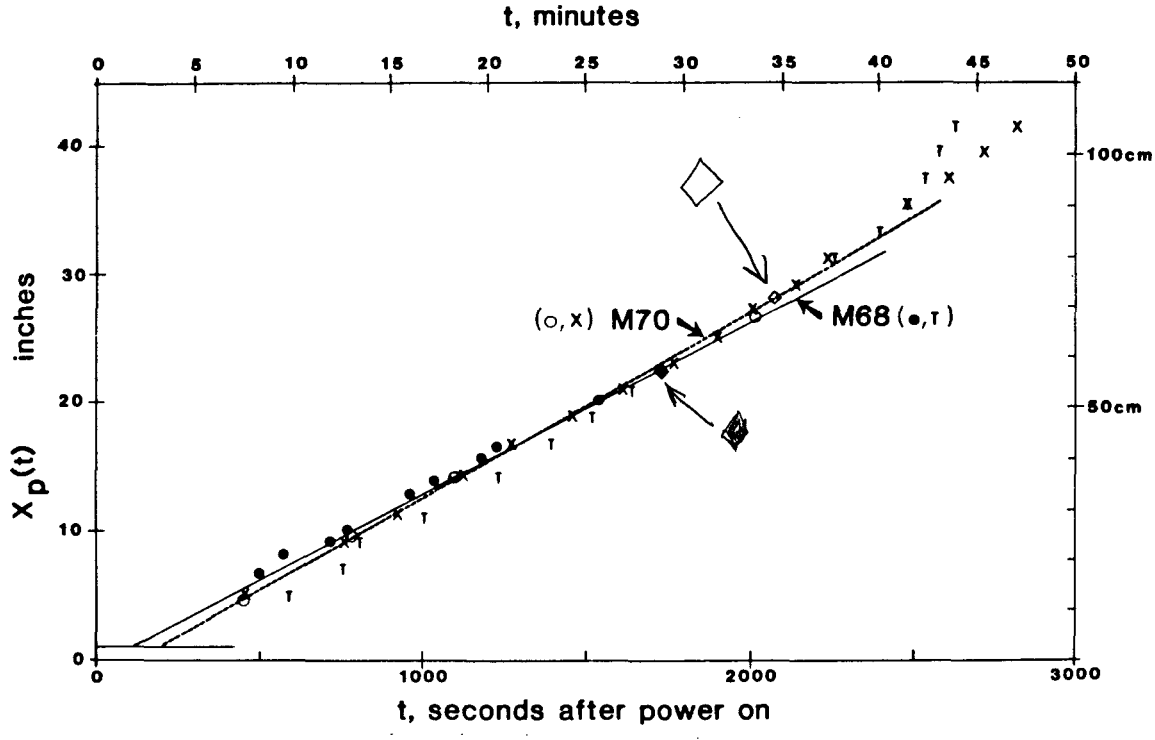

Figure 5. Pool positions $x_p(t)$ above stool for M 68, M 70. Thermocouple trace offset times from assembly process of Figure 4 have been related to clock time by eq. (4); i.e., $x_p(t)$ lines are required to pass through L_f values (diamonds). Thermal data indicated by X,T symbols; ram position data indicated by circles. Horizontal line near origin indicates striker block height h_{st} = 2.5 cm (1 in).

Although no formal error analysis was carried out, it is estimated that the error in placing any one segment of data $T_i(t)$ with respect to the composite $T_c(t^*)$ curve is less than 30 seconds in time. This corresponds to a pool position $x_p(t)$ uncertainty of about 1 cm; i.e., about the thickness of the crucible wall (1.27 cm).

With temperature rise $T_c(t^*)$ determined in this manner, the distribution along the wall can be prescibed by defining $x=U_I(t^*-t^*_{A1})$ to be the distance going down from the pool surface (cm) when t^*_{A1} is the arrival time of the pool at thermocouple 1. Then, if a film coefficient h(T) is given for the heat transfer from the Cu wall to the coolant, the heat flux (and thus the normal derivative $(\partial T/\partial y)$ can be given on the y = 0 surface in Figure 2:

$$-k \frac{\partial T}{\partial y} (x,0) = h(T) \quad (T(x,0) - T_\infty(x)) = h\, T_c(x). \tag{6}$$

Because the water-Glycol coolant is not clean, it was not expected that its film coefficient h(T) when flowing over Cu would be particularly well predicted by standard values. Thus, values were assigned by the following procedure. First, total wall flux was required to be:

$$P_{cool} = 2\pi R_o \int_{-\infty}^{\infty} h(T)\, T_c(x)\, dx, \tag{7}$$

where R_o = 1/2(crucible OD) and P_{cool} is the power being removed by the coolant. This must be related to the coolant flowrate and temperature rise by:

$$P_{cool} = \dot{m}_{cool} C_p\, (T_{out} - T_{in}). \tag{7a}$$

Finally, the temperature dependence of h(T) was required to be the same as the temperature dependence of the film coefficient for saturated (incipient boiling) water, in order that the significant fluxes which occur at the maximum temperature rise, be well treated; i.e.,

$$h(T) = \beta h_{H_2O}(T), \tag{7b}$$

is required, with $h_{H_2O}(T)$ being a standardized value (6). Then β comes from simultaneous use of eqs. (7), on the actual measured quasisteady interval (x_{min}, x_{max})

$$\beta \int_{x_{min}}^{x_{max}} h_{H_2O}(T)\, T_c(x)\, dx = \frac{\dot{m}_{cool} C_p (T_{out} - T_{in})}{2\pi R_o}. \tag{8}$$

This relation ignores heat losses from the coolant piping between thermocouple stations. Since the coolant power derived in this way constitutes more than 90 percent of the electrical input power and the ingot carries off sensible heat, this assumption is felt to be justified. As seen from the abscissae in Figure 4 and the U_I values from Figure 5, the interval length $(x_{max} - x_{min})$ was 132 cm for M 68 and 144 cm for M 70. The resulting β value derived in this way is about 15 percent greater for M 70 than for M 68. It will be argued later that this should have been nearer a 25 percent difference due to differences in interval length and coolant flow velocity, and β for M 68 adjusted accordingly.

From the arrival times of Figure 5 and the assembled thermocouple traces in Figure 4, and "average" composite for the quasisteady temperature is derived and displayed in Figure 6. The averaging for M 68 consists of applying the ram travel $x_p(t)$ arrival times to the assembly process and then doing a simple arithmetic average at each sample time. This gives the broader pulse shape in Figure 6, and the higher peak as well. For M 70, the strongly defined pulse shape near the inside of the data plotted in Figure 4(b) was used to define $T_c(x)$; i.e., the temperature increases on the leading edge of the pulse were ignored.

With the temperature rise pulses aligned as in Figure 6, it is quite apparent that M 68 did not capture as much of the below-pool curve as did M 70. In fact, extending the M 68 pulse roughly parallel to the M 70 pulse so that both end near 50 cm below the pool would enclose about 15 percent more area than the present M 68 curve encloses. That is, the integral appearing on the left hand side of eq. (8) should have about 15 percent more area than it now has, if M 68 and M 70 are to be comparable.

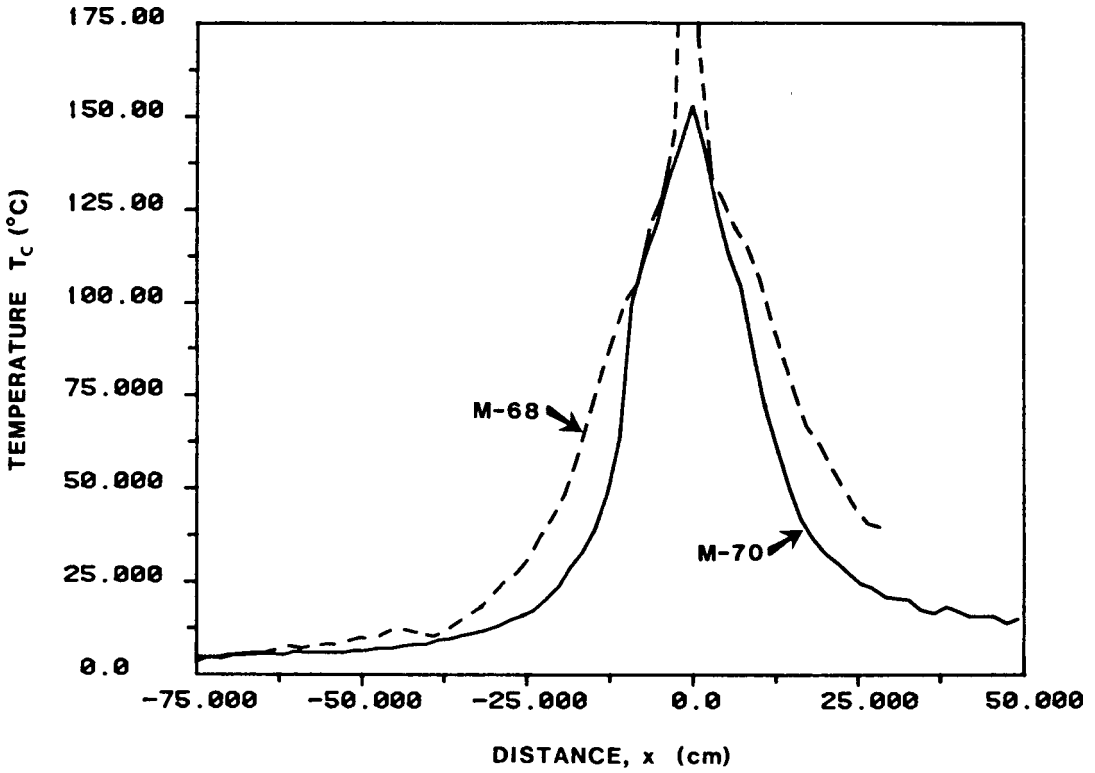

Figure 6. Quasisteady temperature rise $T_c(x)$ (°C) as a function of distance x (cm) below pool surface. Composite for M 68 is the broken curve; M 70 curve lies almost entirely within. Time scale of Figure 4 is converted to $x = U_I(t^* - t^*_{Al})$ with t^*_{Al} being the arrival time of the pool on the time scale used for the origin of t*. Note that the pool position is very close to the peak temperature point.

Increasing the integral in this manner would decrease the film coefficient by another 15 percent below the β value of M 70. Since heat transfer varies as $(\text{velocity})^{0.8}$ (see Ref. 6, p. 7-32), it would be expected that $\beta_{68} \sim \beta_{70}/(90/50)^{0.8} \sim 0.64\ \beta_{70}$ if all else were constant. This is nearly the value produced by this 15 percent adjustment of the length of the M 68 data, so it is adopted.

Another view of the same data is given in Figure 7. The cumulative fraction $\alpha(x)$ of the coolant power collected above station x is shown there as a function of x. This fraction for ideal quasisteady conditions is defined in the caption of Figure 4; the actual value plotted in Figure 7 is:

$$\alpha(x) = \int_{x_{min}}^{x} h(T)\ T_c(x)\ dx \Big/ \int_{x_{min}}^{x_{max}} h(T)\ T_c(x)\ dx.$$

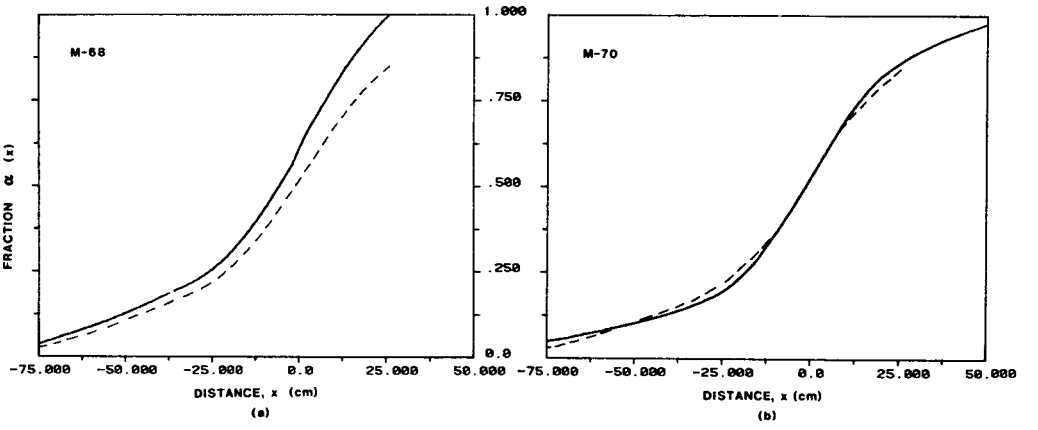

Figure 7. Cumulative power deposition fraction $\alpha(x)$ as a function of distance x(cm) below pool surface, for (a) M 68 and (b) M 70. Broken line in each plot is $0.85\ \alpha_{68}(x)$, adjusted for shorter duration of M 68. Note that adjusted values are not distinguishable from M 70 values, indicating the same spatial distribution of energy in the two arcs.

The extremely close agreement of the $\alpha(x)$ curves for M 70 and adjusted M 68 in Figure 7 indicates that the somewhat diffused form of the power deposition profile seen on the outside of the crucible wall is essentially the same for the two melts. Both have about half the power deposited above the pool and the remaining half below.

The inverse heat flow boundary value problem defined in Figure 2 can now be completed. On the y = 0 surface, the temperature difference $T_c(x)$, with the x origin shifted so that $0 \leq x \leq L$ as in Figure 2, is specified, and the normal derivative is given by eq. (6) using the β value from eq. (8). On the ends x = 0 and x = L, constant temperatures are specified:

$$T(0,y) = T_c(x_{min}) = T_1 \text{ and } T(L,y) = T_c(x_{max}).$$

Next, temperature $T_3(x,y)$ is defined as the temperature distribution in the slab which gives zero on each surface of the slab except the right hand end, where $T_3(L,y) = T_c(x_{max}) - T_1$. Then the formal solution to eq. (3) can be written down:

$$T(x,y) = T_1 + T_3(x,y) + e^{-U_I x/2\kappa} \sum_{k=1}^{\infty} G_k \cosh \alpha_k \frac{y}{H} + F_k \frac{\sinh \alpha_k \frac{y}{H}}{\alpha_k/H} \sin k\pi \frac{x}{L} \qquad (9)$$

where $\alpha_k^2 = \frac{Pe^2}{4} + \frac{H^2}{L^2}(k\pi)^2$ and $Pe = \frac{U_I H}{\kappa}$ is the Peclet number based on wall thickness, H. In these experiments, Pe ~ 0.05, indicating a conduction dominated solution. However, as has already been seen in Figure 4, the length scale of the energy deposition is comparable to the advection-diffusion length scale (scale of the exponential term in eq. (9)), so both features of the solution (9) must be retained.

The coefficients G_k and F_k in eq. (9) are simply the Fourier coefficients:

$$G_k = \frac{2}{L} \int_0^L e^{U_I x/2\kappa} \left(T_c(x) - T_3(x,0) - T_1\right) \sin k\pi \frac{x}{L} \, dx \qquad (9a)$$

and

$$F_k = \frac{2}{L} \int_0^L e^{U_I x/2\kappa} \left(\frac{h(T)}{k} T_c(x) - \frac{\partial T_3}{\partial y}(x,0)\right) \sin k\pi \frac{x}{L} \, dx \qquad (9b)$$

It follows that these can be found very rapidly by a Fast Fourier Transform (FFT), provided that the interval (0,L) is divided into N = 2^n subintervals, where n is an integer. Similarly, the series in eq. (9) can be evaluated by FFT once the y-dependent coefficients are evaluated. The efficiency of FFT calculations is such that the minicomputer used for data logging was also adequate for solving the inverse heat flow problem.

The solution (9) is viewed as purely a formal solution because it cannot be evaluated for infinite k due to the unboundedness of the cosh $\alpha_k y$ and $\sinh\alpha_k y$ terms. Both these terms behave like exp ($\alpha_k y$) at large values of the argument. No matter how small y may be, if it is nonzero, ($\alpha_k y$) can be made arbitrarily large by taking a sufficiently large k value. This means that the inverse heat flow problem is ill-posed in the sense of Hadamard, because infinitesimal noise in the coefficient of infinitely large k terms can result in solutions with nearly identical data being indefinitely far apart.

The problem then is regularization of the violent series (9); see, e.g., Ref. (7) for a full discussion. Here, the simplest regularization is used--solutions are computed at N values chosen by trial and error. When the "spikiness" of the solution due to errors in the large-k (i.e., high spatial frequency) terms threatens to swamp the solution, no further increase of N is attempted. The result, as shown in Figure 8, is that 32 points in the interval (0,L) are used as working resolution.

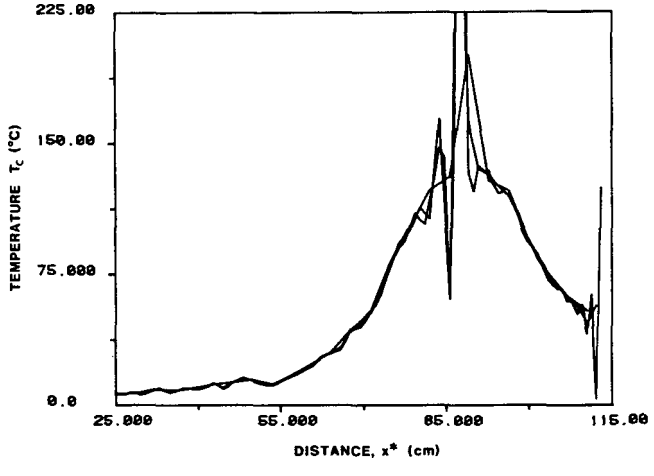

Figure 8. Heuristic determination for M 68 of truncation point for series solution eq. (9). Curves show inside temperature difference as a function of x^* (difference, cm). Solutions are shown for N = 32, 64, and 128. Each increase of N is accompanied by increased high frequency "ringing" of the solution, so N = 32 is chosen as working resolution for M 68 and M 70 data.

When eq. (9) is evaluated its derivative $\partial T/\partial y$ can also be evaluated, giving the flux along with the temperature at the chosen y value. The resulting inside (y = H) heat flux distributions are given in Figure 9.

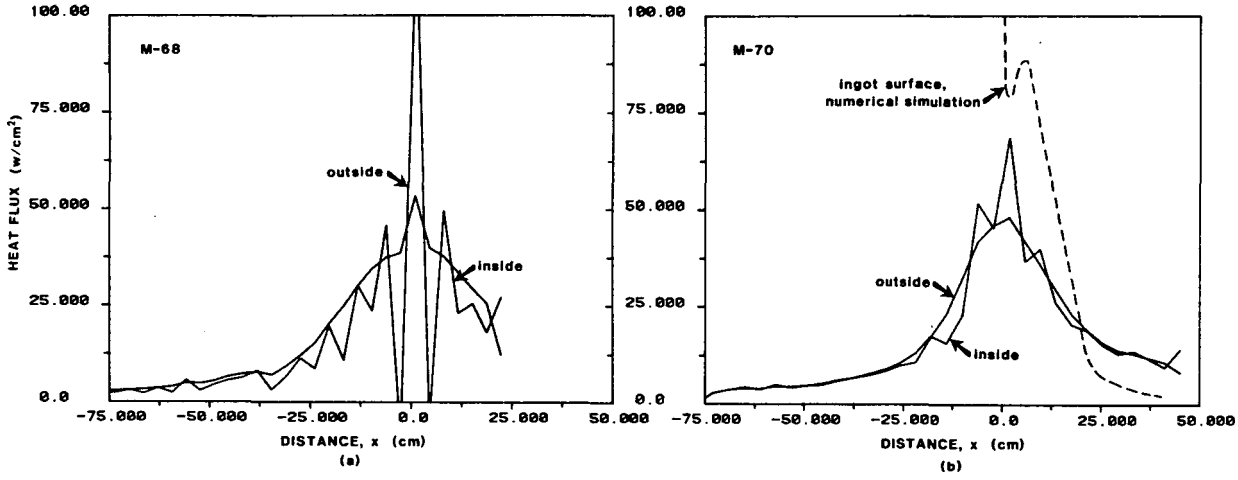

Figure 9. Heat flux (W/cm^2) vs distance x (cm) below pool for (a) M 68 and (b) M 70. Smooth solid curves are outside crucible wall fluxes given by eq. (6); jagged solid curves are inside fluxes obtained from eq. (9) using N = 32 points in FFT. Broken curve in (b) is ingot lateral surface flux as obtained by numerical simulation described in Refs. (1) and (2). Computational parameters were: 6.0 kA melt current, with 3.3 kA passing through pool; conduction contact ending 200°C below nonequilibrium solidus (1132°C); length of computational zone, 3.5 radii (about 40 cm).

The experimental noise level in the M 68 data is high enough that the inside flux in Figure 9(a) displays considerable "ringing" even at N = 32 points. Nevertheless, its general trend is apparent: the above-pool curve is narrower while the below-pool curve is essentially the same as the outside flux distribution curve. For M 70, the same qualitative observation can be made with greater confidence, as there is much less distortion of the curve by high frequency misbehavior.

During M 68, thermocouple data were returned from inside the crucible as well as from outside. The sheaths of the inside thermocouples apparently buckled out of their milled grooves during the melt, since segments of the sheaths wound up imbedded in the ingot. Apparently this buckling was due to differential expansion coefficients of Ta and Cu or due to heating of the sheaths on one side, cooling on the other. In any event, as can be seen in Figure 10, the buckling did not prevent return of accurate inside temperature until about the time of pool arrival. After that time, the temperature seen by the inside thermocouple was apparently some ambiguous combination of crucible wall temperature and ingot lateral surface temperature, so no attempt is made to interpret it.

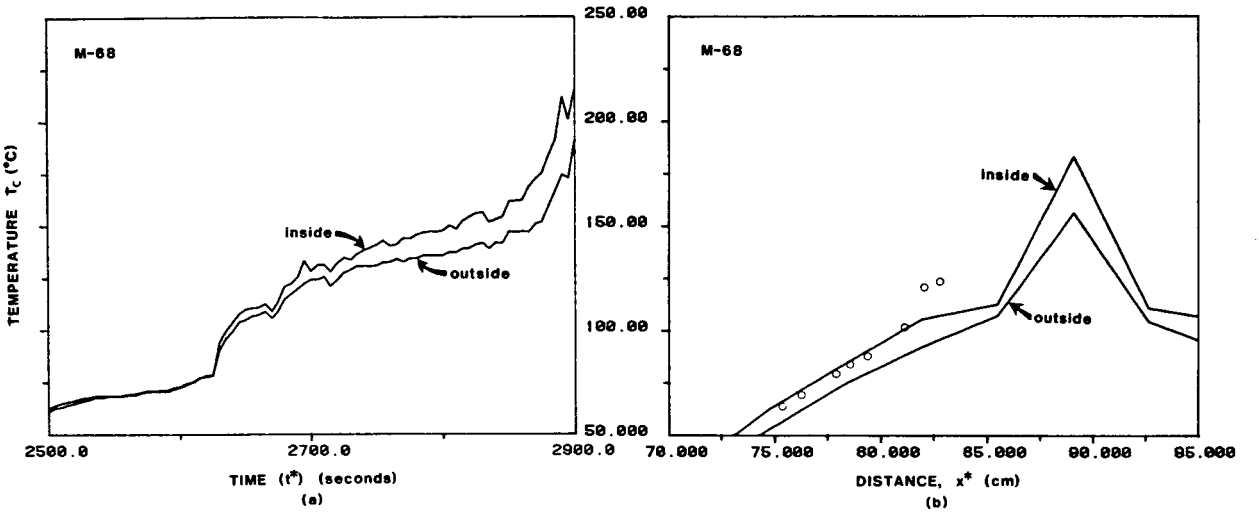

Figure 10. (a) Inside (upper) and outside (lower) thermocouple temperature histories at 13.03 in (33.1 cm) above stool in M 68. Steep rise in temperature at about 2630 s is due to thermal transient associated with a ram short; close coincidence of this and other features on the two traces is taken to indicate realistic inside data. (b) Inside (upper: from eq.(9)) and outside (lower; from Fig. 6) composite temperatures as a function of distance (cm); pool at 88 cm on this scale. Circles are temperature differences from Figure 10 (a) added to outside temperature curve $T_c(x)$. If predicted inside temperature were exact and measurement were truly quasisteady, circles would presumable lie on inside temperature curve. The general agreement seen here can only be considered qualitative because of boiling of coolant and uncertain differential calibrations of thermocouples.

Results and Conclusions

The results obtained here are not of sufficient resolution to define boundary conditions on the ingot below a 1 cm scale. At and above this scale, useful bounds on energy partition have been determined. Further refinement should extend these preliminary results to smaller scales. In the above analysis, most of the high noise levels in the thermocouple data were attributed to coolant boiling. This boiling was enhanced in M 68 by (i) a low coolant flowrate, (ii) large interference with coolant flow by thermocouple leads and hold-down tapes, and (iii) furnace ram short transients caused by gap/ingot length measurements. These problems were reduced in M 70 by use of a nearly doubled flowrate, cleaner lead retainers and less frequent ram shorts. Nevertheless, large thermal excursions were observed downstream of the pool position during ram shorts, causing the overshoots of temperature on the leading edge of the M 70 pulse in Figure 4(b).

With these systematic sources of noise identified, appropriate signal conditioning could be applied to give the best resolution supportable by the data and the FFT analysis. This resolution is about ± 30 s in time, ± 1 cm in space for pool position.

Within this resolution, the quasisteady pulse shapes were determined for the nominally identical melts M 68 and M 70. These shapes indicate significant flux extends from nearly 75 cm above the pool to nearly 75 cm below it; recall

Figure 6. About half this flux is deposited above the pool as seen in Figure 7. Most of this deposition must come from plasma and neutral metal vapor produced by the arc processes, since radiation from molten surfaces and splatter of liquid metal can together account for only about 15 kW of the 65-75 kW of deposition implied by this 50-50 partition (2), (9).

The half of the coolant power captured below the pool surface is apparently quite smoothly and reproducibly distributed (Figure 9). Since this below-pool flux and temperature distribution is the direct result of the pool-ingot boundary condition, this reproducibility is encouraging to the numerical simulation effort. Less encouraging is the observed length scale of this distribution--50-75 cm below the pool is required to capture all the significant flux. This corresponds to 5-7 radii, and implies that quite long computational zones are required to correctly simulate the thermal conditions near the ingot top. The present simulation produces an ingot surface flux distribution like the broken line curve in Figure 9(b), with much shorter length scale than this. This discrepancy suggests that the parameters of the simulation model, derived in a totally independent way (1), (2), should be adjusted.

Although quite efficient, the FFT calculations are too inflexible to allow fine tuning for extraction of maximum information from this data. The major inflexibility is the $N = 2^n$ requirement on mesh size, and reinforcing this, our practice of using simple truncation rather than some further signal conditioning on high-frequency data. Future analysis will explore improvements of these features.

The quantitative results can be summarized and compared to previous work (8) in the following table.

	M 68	M 70	Y-12 (Ref. 8)
I_m, kA	6.0	6.0	6.0
p, microns	2-8	2-8	NA
V_m, V	25	27	28
P_{cool}/I_mV_m	0.92 $\pm$ 0.05	0.91 $\pm$ 0.04	0.89
Power above pool, %	52	52	NA
U_I, cm/s	0.033	0.036	0.034
$\dot{m}$, g/s	182	192	206

Table I. Melting parameters for experiments reported here (M68 and M70) as well as earlier experiment done jointly with Union Carbide Y-12 (Ref. 8). Measured quantities are melt current I_m; crucible ambient gas pressure, p; furnace voltage V_m; fraction of input power removed by coolant, P_{cool} solidus I_mV_m; fraction of coolant power deposited on crucible above pool surface; growth rate of ingot, U_I; melt rate of electrode, $\dot{m}$, respectively.

Acknowledgement

Throughout the course of this investigation, significant contributions to data acquisition have been made by J. Maroone of Sandia National Laboratories, and to data analysis by D. Melgaard of J&M Associates. Assistance in obtaining material, metallurgical analysis, and melting was extended by Y-12 personnel J. Koger, D. Beck, N. Jessen, and G. Northcutt.

References

1. L. A. Bertram and F. J. Zanner, "Interaction Between Computational Modeling and Experiments for Vacuum Consumable Arc Remelting," pp. 333-349 in Modeling of Casting and Welding Processes, H. D. Brody and D. Apelian, eds. AIME, New York, NY, 1981.

2. L. A. Bertram and F. J. Zanner, "Plasma and Magnetohydrodynamic Problems in Vacuum Arc Remelting," in Metallurgical Applications of Magnetohydrodynamics, M. R. E. Proctor, ed. The Metals Society, London (to appear).

3. F. J. Zanner, "Metal Transfer During Vacuum Consumable Arc Remelting," Sandia National Laboratories Report SAND77-1410, Albuquerque, NM, 1977.

4. F. J. Zanner, "Vacuum Consumable Arc Remelting Electrode Gap Control Strategies Based on Drop Short Properties," Metallurgical Transactions, 12B (1981), pp 721-728.

5. Fundamentals Handbook, ASME 1977, New York, NY, pp 17-7 and 17-8.

6. Handbook of Heat Transfer, W. M. Rohsenow and J. P. Hartnett, eds. Mcgraw-Hill, New York, NY, 1973, pp 2-58 and 7-92.

7. V. I. Lavrientiev, Improperly Posed Problems of Mathematical Physics, Springer-Verlag, New York, NY, 1973.

8. F. J. Zanner and L. A. Bertram, "Computational and Experimental Analysis of a U-6w/o Nb Vacuum Consumable Arc Remelted Ingot," Sandia National Laboratories Report SAND80-1156, Albuquerque, NM, 1981.

9. F. J. Zanner and L. A. Bertram, "Behavior of Sustained High Current Arcs on Molten Alloy Electrodes During Vacuum Consumable Arc Remelting," in Proceedings of Xth International Symposium on Discharges and Electrical Insulation in Vacuum, IEEE Catalog No. 82CH1826-7, New York, NY, 1982, pp 353-367.